Chapter I

Coherent dynamics of Mn-doped positively charged quantum dots

I.1 Mn in a II-VI positively charged quantum dot

Cf Optical control of the spin of a magnetic atom in a semiconductor QD, L. Besombes et. al., Sept 2014

I.1.1 Spin structure of a positively charged Mn doped quantum dot

Cf XplusMnRes.pptx to detail the e-Mn levels

E included in model for generality (cite Claire paper "Resonant pumping..." [1]). The effects will be discussed in depth later.

As presented in Sec. ??, a Mn atom in a strained self-assembled CdTe QD exhibits a fine structure dominated by a weak magnetic anisotropy with an easy axis along the QD axis. Neglecting the tetrahedral crystal field of the CdTe matrix, this fine structure is described by the effective spin Hamiltonian

$$\mathcal{H}_{Mn,CF} = D_0 S_z^2 + E(S_y^2 - S_x^2) \tag{I.1}$$

with D_0 depicting the effect of the biaxial strain and E describing the anisotropy of the strain in the plane of the QD. It was shown that the anisotropy of strain was essential to understand the absence of pumping for Mn in strain-free quantum dots [1] and was thus include here to keep generality. We will study more in details its effect on Sec. I.2.

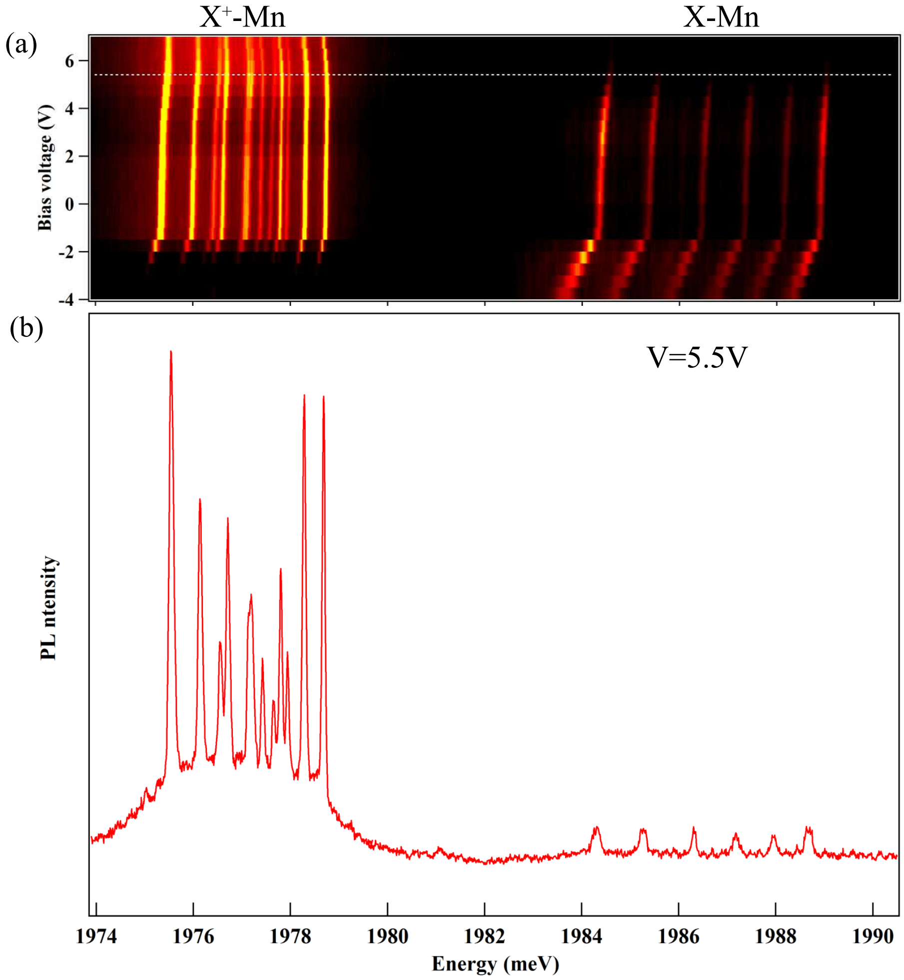

Figure I.1: (a) Color scale plot of the PL intensity of the studied Mn doped QD inserted in Schottky structure showing the emission of the neutral (X-Mn) and positively charged (X^+-Mn) exciton as a function of energy and bias voltage. (b) PL of the Mn-doped QD under a positive bias voltage of V=5.5V.

Nulla malesuada porttitor diam. Donec felis erat, congue non, volutpat at, tincidunt tristique, libero. Vivamus viverra fermentum felis. Donec nonummy pellentesque ante. Phasellus adipiscing semper elit. Proin fermentum massa ac quam. Sed diam turpis, molestie vitae, placerat a, molestie nec, leo. Maecenas lacinia. Nam ipsum ligula, eleifend at, accumsan nec, suscipit a, ipsum. Morbi blandit ligula feugiat magna. Nunc eleifend consequat lorem. Sed lacinia nulla vitae enim. Pellentesque tincidunt purus vel magna. Integer non enim. Praesent euismod nunc eu purus. Donec bibendum quam in tellus. Nullam cursus pulvinar lectus. Donec et mi. Nam vulputate metus eu enim. Vestibulum pellentesque felis eu massa.

Quisque ullamcorper placerat ipsum. Cras nibh. Morbi vel justo vitae lacus tincidunt ultrices. Lorem ipsum dolor sit amet, consectetuer adipiscing elit. In hac habitasse platea dictumst. Integer tempus convallis augue. Etiam facilisis. Nunc elementum fermentum wisi. Aenean placerat. Ut imperdiet, enim sed gravida sollicitudin, felis odio placerat quam, ac pulvinar elit purus eget enim. Nunc vitae tortor. Proin tempus nibh sit amet nisl. Vivamus quis tortor vitae risus porta vehicula.

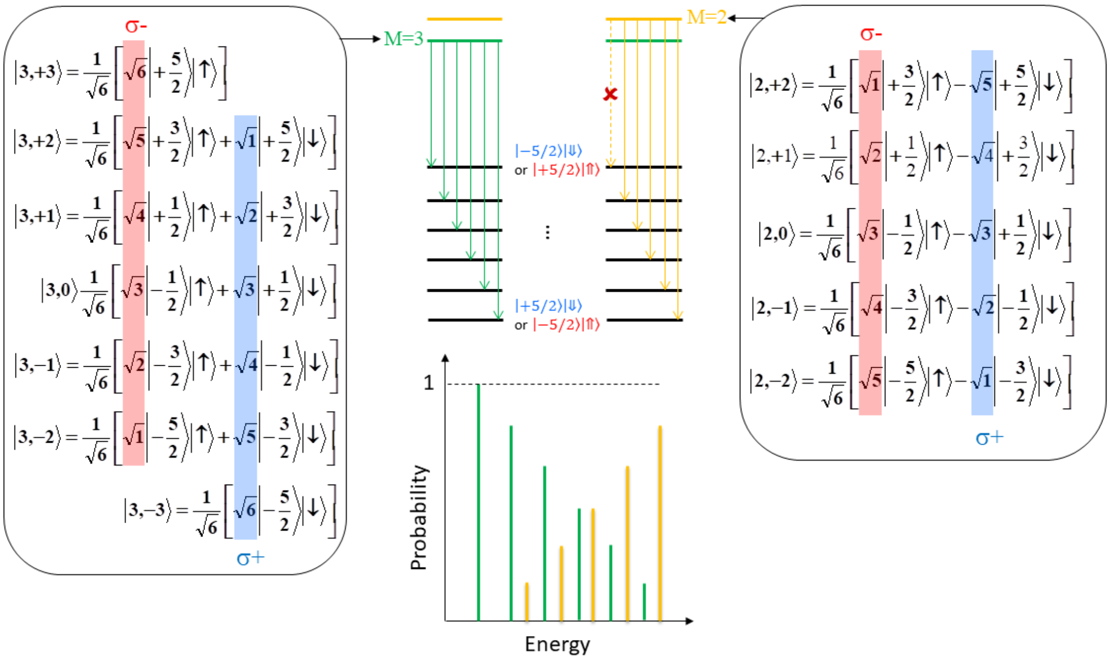

Figure I.2: Electron-Mn spin states for each $|M, M_z\rangle$. For each M, the $\sigma-$ (red) and $\sigma+$ (blue) probability is highlighted. This probability is directly linked to the intensity of each peak. In the center, the different possible recombination path for $M = 3$ and $M = 2$ are presented. A schema of the resulting spectra is drawn below.

Fusce mauris. Vestibulum luctus nibh at lectus. Sed bibendum, nulla a faucibus semper, leo velit ultricies tellus, ac venenatis arcu wisi vel nisl. Vestibulum diam. Aliquam pellentesque, augue quis sagittis posuere, turpis lacus congue quam, in hendrerit risus eros eget felis. Maecenas eget erat in sapien mattis porttitor. Vestibulum porttitor. Nulla facilisi. Sed a turpis eu lacus commodo facilisis. Morbi fringilla, wisi in dignissim interdum, justo lectus sagittis dui, et vehicula

Table I.1: Values of the parameters used in the model of the positively charged Mn-doped QD presented in Fig. I.1. I_{eMn}, I_{hMn}, $\frac{\rho_s}{\Delta_{lh}}$, θ, η and T_{eff} are used to model the linear polarization intensity map of Fig. I.3. The other parameters cannot be extracted from the PL measurements and values for typical Mn-doped QDs are chosen for the calculation of the spin dynamics presented in Sec. I.2 and I.3.

I_{eMn}	I_{hMn}	$\frac{\rho_s}{\Delta_{lh}}$	θ	η	T_{eff}	g_e	g_h	g_{Mn}	D_0	E
μeV	μeV		$\circ$	μeV	K				μeV	μeV
-175	345	0.09	0	30	20	-0,4	0.6	2	7	1.5

libero dui cursus dui. Mauris tempor ligula sed lacus. Duis cursus enim ut augue. Cras ac magna. Cras nulla. Nulla egestas. Curabitur a leo. Quisque egestas wisi eget nunc. Nam feugiat lacus vel est. Curabitur consectetuer.

Sed commodo posuere pede. Mauris ut est. Ut quis purus. Sed ac odio. Sed vehicula hendrerit sem. Duis non odio. Morbi ut dui. Sed accumsan risus eget odio. In hac habitasse platea dictumst. Pellentesque non elit. Fusce sed justo eu urna porta tincidunt. Mauris felis odio, sollicitudin sed, volutpat a, ornare ac, erat. Morbi quis dolor. Donec pellentesque, erat ac sagittis semper, nunc dui lobortis purus, quis congue purus metus ultricies tellus. Proin et quam. Class aptent taciti sociosqu ad litora torquent per conubia nostra, per inceptos hymenaeos. Praesent sapien turpis, fermentum vel, eleifend faucibus, vehicula eu, lacus.

I.1.2 Optical Λ-level identification

Sed feugiat. Cum sociis natoque penatibus et magnis dis parturient montes, nascetur ridiculus mus. Ut pellentesque augue sed urna. Vestibulum diam eros, fringilla et, consectetuer eu, nonummy id, sapien. Nullam at lectus. In sagittis ultrices mauris. Curabitur malesuada erat sit amet massa. Fusce blandit. Aliquam erat volutpat. Aliquam euismod. Aenean vel lectus. Nunc imperdiet justo nec dolor.

Etiam euismod. Fusce facilisis lacinia dui. Suspendisse potenti. In mi erat, cursus id, nonummy sed, ullamcorper eget, sapien. Praesent pretium, magna in eleifend egestas, pede pede pretium lorem, quis consectetuer tortor sapien facilisis magna. Mauris quis magna varius nulla scelerisque imperdiet. Aliquam non quam. Aliquam porttitor quam a lacus. Praesent vel arcu ut tortor cursus volutpat. In vitae pede quis diam bibendum placerat. Fusce elementum convallis neque. Sed dolor orci, scelerisque ac, dapibus nec, ultricies ut, mi. Duis nec dui quis leo sagittis commodo.

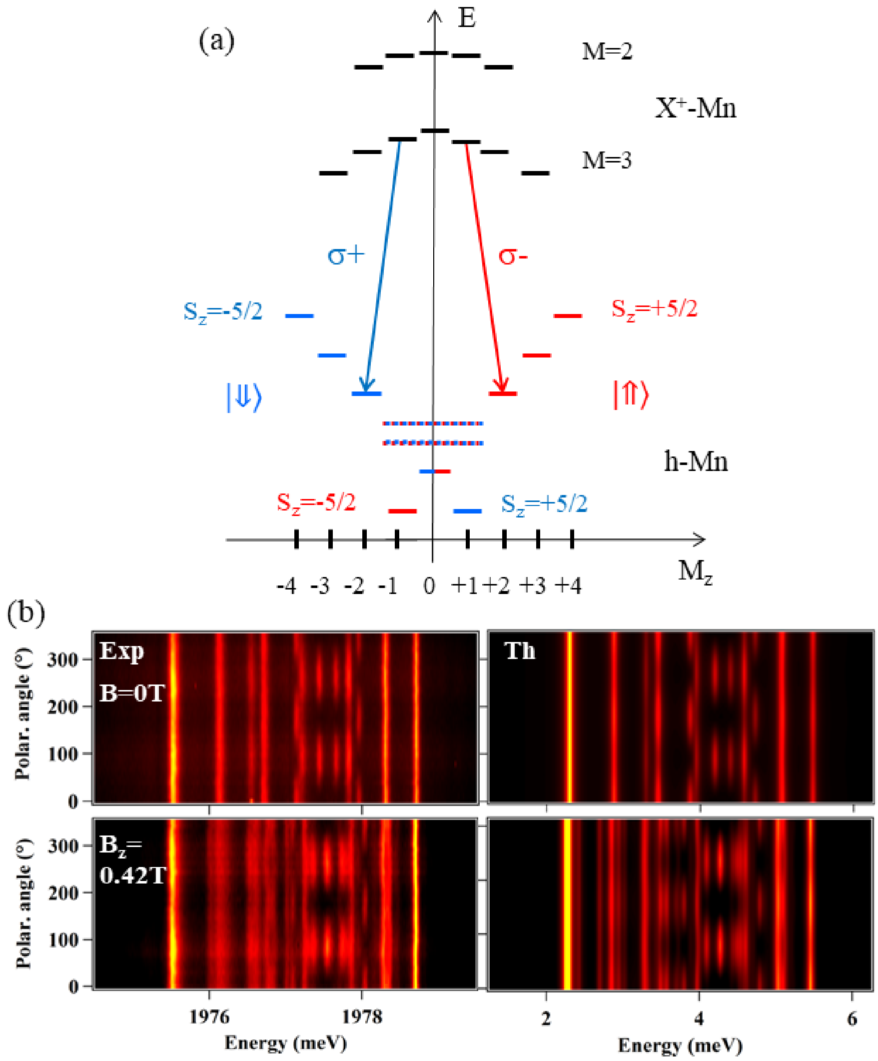

Figure I.3: (a) Energy levels of the ground (h-Mn) and excited (X^+-Mn) states as a function of their angular momentum (M_z). The levels in dotted lines corresponds to the h-Mn states $|-1/2\rangle|\Uparrow\rangle$ and $|+1/2\rangle|\Downarrow\rangle$ coupled by the valence band mixing. Optical recombination towards these levels leads to the linearly polarized lines observed in (b). (b) Experimental (left) and calculated (right) color-scale plot of the linear polarization dependence of the PL of X^+-Mn at $B = 0$ T (top) and $B_\perp = 0.42$ T (bottom). The parameters used in the calculation are listed in Table I.1.

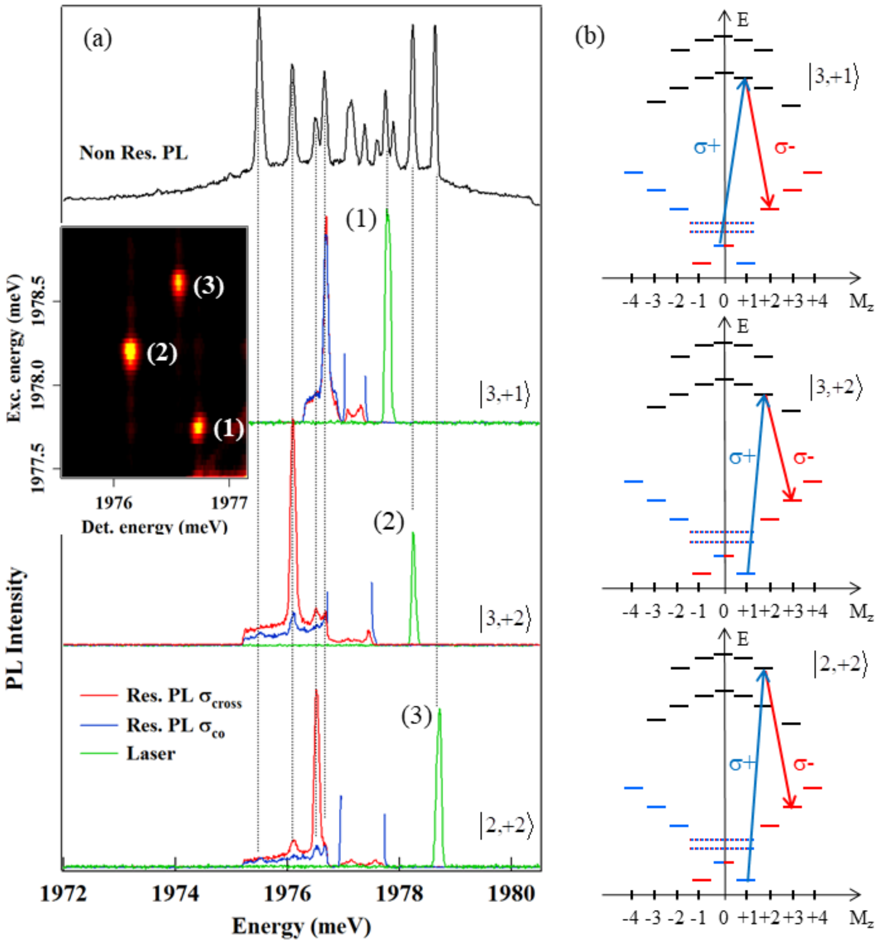

Figure I.4: (a) Non resonant (Non Res.) and resonant (Res.) PL of X^+-Mn. Co and cross circularly polarized PL spectra are collected for three different energies of the CW resonant laser (green). Inset: intensity map of the cross-circularly polarized PL detected on the low energy side of X^+-Mn as the CW laser is scanned through the high energy side. (b) Energy levels of X^+-Mn and identification of the three resonances observed in (a) corresponding to the optical Λ systems associated with the e-Mn states $|3,+1\rangle$, $|3,+2\rangle$ and $|2,+2\rangle$.

I.2 Spin dynamics under resonant excitation

Cf article 2016/01

I.2.1 Cycling and escaping the λ-level system

Under resonant excitation of one high energy level of X^+-Mn, only one cross-circularly polarized emission line is observed. It corresponds to the optically allowed recombination on the second branch of the Λ system. This recombination occurs with a flip-flop of the electron and Mn spins [2]. The energy splitting between the resonant absorption and the emission corresponds to the splitting between the two ground states of the Λ system. It is given by $4\times3/2I_{hMn}$($\approx$2.1 meV for the studied QD) for an excitation of $|3,+2\rangle$ or $|2,+2\rangle$ and $2\times3/2I_{hMn}$($\approx$1.05 meV for the studied QD) for an excitation of $|3,+1\rangle$. For an excitation of $|3,+2\rangle$ or $|2,+2\rangle$, the weak co-polarized PL signal, which depends on the excitation intensity, comes from a possible direct excitation of the low energy branch of the Λ system through the acoustic phonon side-band [3].

For an isolated Λ system, under resonant excitation of one of the branch, a fast optical pumping controlled by the generation rate and the radiative lifetime of the excited state is expected: The population is expected to be stored in the level which is not excited and the resonant PL should vanish. In the case of X^+-Mn, the PL intensity observed under resonant excitation of the high energy branch of the Λ systems is similar to the PL intensity obtained under non-resonant excitation. This suggests a very inefficient optical pumping of the Mn-hole spin and an efficient spin-flip mechanism which links the two ground states of the Λ systems.

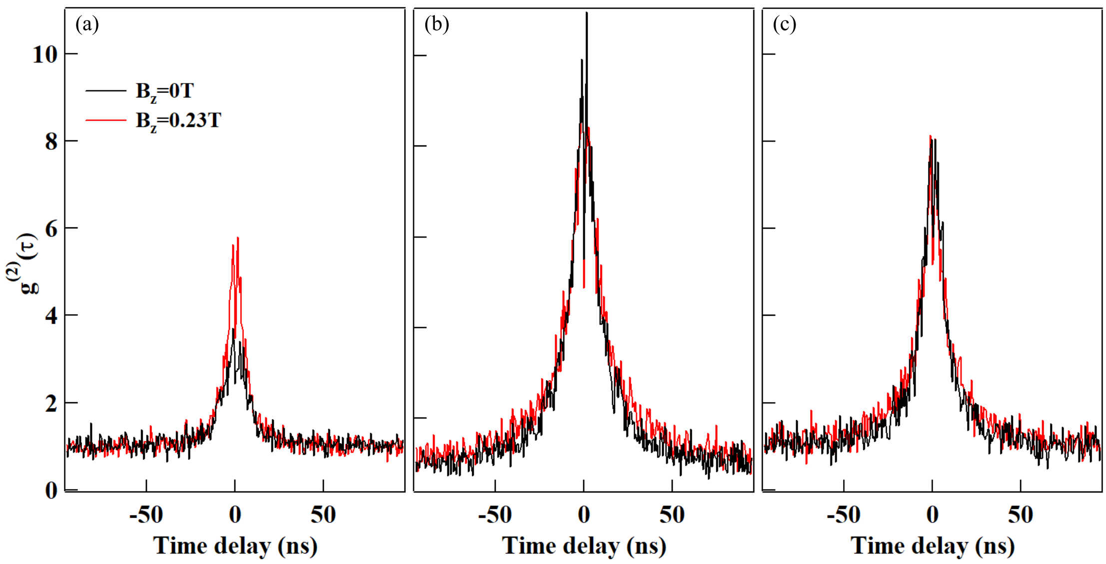

Figure I.5: Auto-correlation of the resonant PL for cross-circularly polarized excitation and detection of the electron-Mn states (a) $|3,+1\rangle$, (b) $|3,+2\rangle$ and (c) $|2,+2\rangle$.

The dynamics of the Mn spin coupled to carriers was first analyzed, under resonant optical excitation, through the statistics of the time arrival of the photons given by the second order correlation function of the resonant PL intensity, $g^{(2)}(\tau)$. For the three resonant excitation conditions reported in Fig.I.5, $g^{(2)}(\tau)$ is mainly characterized by a large photon bunching with a full width at half maximum (FWHM) in the 20 ns range. The amplitude of the bunching reaches 9 for line (2) and is slightly weaker for the two other lines. This large bunching, reflecting an intermittency in the emission of the QD, is not sensitive to a longitudinal magnetic field B_z except for an excitation on (1).

The presence of a photon bunching is at first sight surprising: under resonant excitation of an isolated Λ system, an anti-bunching of the resonant PL controlled by the transfer time between the two ground states is indeed expected. For X^+-Mn, the observed short anti-bunching (dip near zero delay, better evidenced in Fig. I.5 (b)) suggests a fast transfer time in the nanosecond range between the two ground states of the Λ systems.

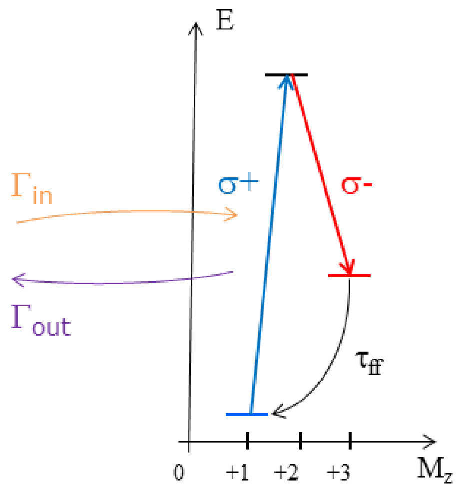

Figure I.6: Schema of the energy levels of the optical Λ system associated with the electron-Mn state $|3,+2\rangle$ extracted from the full level structure of a positively charged Mn-doped QD (Fig. I.4). The different processes discussed in this section are presented on it.

In the presence of a transfer process connecting the two Mn-hole ground states in a nanosecond time-scale, the photon bunching can be explained by leaks outside the resonantly excited Λ system. Under *cw* excitation, the population is cycled inside the Λ system until a spin flip occurs and drives the carrier-Mn spin out of the Λ levels under investigation. The resonant PL is then switched off until multiple spin-flips drives back the carriers and Mn spin inside the Λ system under excitation. The selected QD line can be either in a ON or OFF state depending on the fluctuations of the carrier and Mn spins. The amplitude of the bunching is then given by Γ_{Out}/Γ_{In} the ratio of the transition rates from OFF to ON (Γ_{In}) and from ON to OFF (Γ_{Out}). An amplitude of bunching larger than 1 is expected for the multilevel system considered here where, after a spin relaxation, multiple spin flips are in average required to come back to the initial state ($\Gamma_{In} < \Gamma_{Out}$). Within this picture, the width of the bunching is a measurement of the escape time out of the considered Λ level system. We present these transitions in Fig. I.6, on the Λ system associated with $|3, +2\rangle$ state.

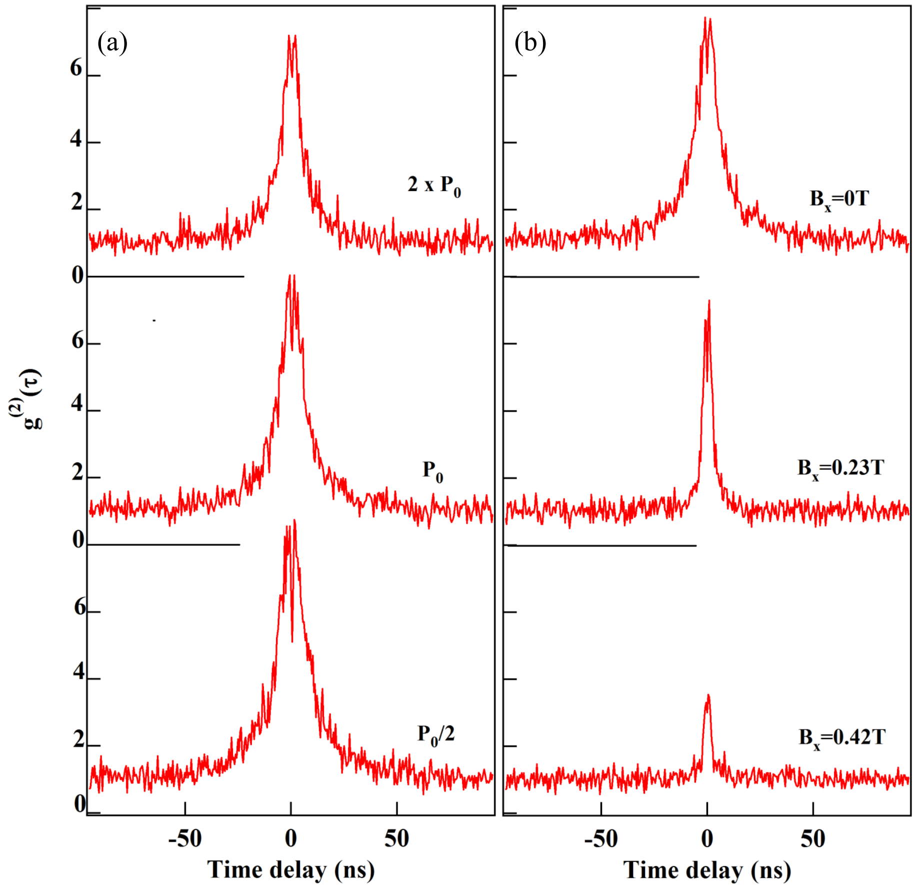

Figure I.7: Excitation power dependence (a) and transverse magnetic field dependence (b) of the auto-correlation of the resonant PL obtained for an excitation on the high energy branch of the Λ level system associated to the e-Mn state $|2, +2\rangle$.

A weak transverse magnetic field, B_x, significantly reduces the width of the bunching signal (Fig.I.7 (b)). As the spin of the Mn-hole complex is highly anisotropic, with a large energy splitting induced by the exchange interaction $I_{hMn}S_z.J_z$, the weak transverse magnetic field mainly affects the electron-Mn dynamics in the excited state of the charged QD. Indeed, the transverse magnetic field couples the different electron-Mn states and induces a leak outside the resonantly excited Λ system. Both spin-flips within the Mn-hole (ground state) and the electron-Mn (excited state) systems can contribute to the bunching signal. The significant effect of the weak transverse field shows that the probability of presence in the excited state of the Λ system is large. This is consistent with the large excitation intensity used for these auto-correlation measurements which require a high photon count rate.

A slight reduction of the width of the bunching signal is also observed with the increase of the excitation power (Fig.I.7 (a)). This shows that the leaks outside a given Λ system slightly increases with the probability of presence of the positively charged exciton in the QD.

Resonant optical pumping experiments were done to estimate how long it takes, after a spin-flip, to the hybrid Mn-hole spin to relax back inside the resonantly excited Λ system. A demonstration of resonant optical pumping of the Mn-hole system was first done by exciting the high energy branch of the Λ systems with trains of resonant light, alternating the circular polarization and recording the circularly polarized PL of the low energy branch. As observed in Fig. I.8, for an excitation on resonance with the electron-Mn states $|3,+2\rangle$ or $|2,+2\rangle$, switching the polarization of the excitation from co to cross circular produces a change of the PL intensity with two transients: first, an abrupt PL increase (or decrease), reflecting the population change of the observed spin-polarized charged excitons; then a slower transient with a characteristic time of a few tens of nanoseconds, depending on the laser excitation power.

The progressive decrease of the resonant PL intensity is the signature of an optical pumping of the Mn-hole spin: the Mn-hole state which is optically addressed is partially emptied when the population is ejected out of the excited Λ system. As presented in Fig. I.8, this pumping signal is not sensitive to a longitudinal magnetic field B_z except for an excitation of $|3,\pm1\rangle$ where a significant intensity difference between co and cross circular polarization is only observed under a weak B_z.

The speed of the optical pumping increases with the excitation intensity. This is presented in Fig. I.9 (a) in the case of a resonant excitation of $|3,\pm2\rangle$ with alternate circular polarization. At high excitation intensity, the pumping time saturates to a value similar to the width of the bunching signal observed in the auto-correlation measurements.

As observed for the auto-correlation, the resonant pumping signal is also strongly sensitive to a transverse magnetic field. Under a weak transverse field (see Fig. I.9 (b)), we first observe an increase of the speed of the pumping together with a decrease of the amplitude of the signal when the transient time reaches the time resolution of the set-up (around 10 ns). For a large transverse field ($B_\perp$=0.42T),

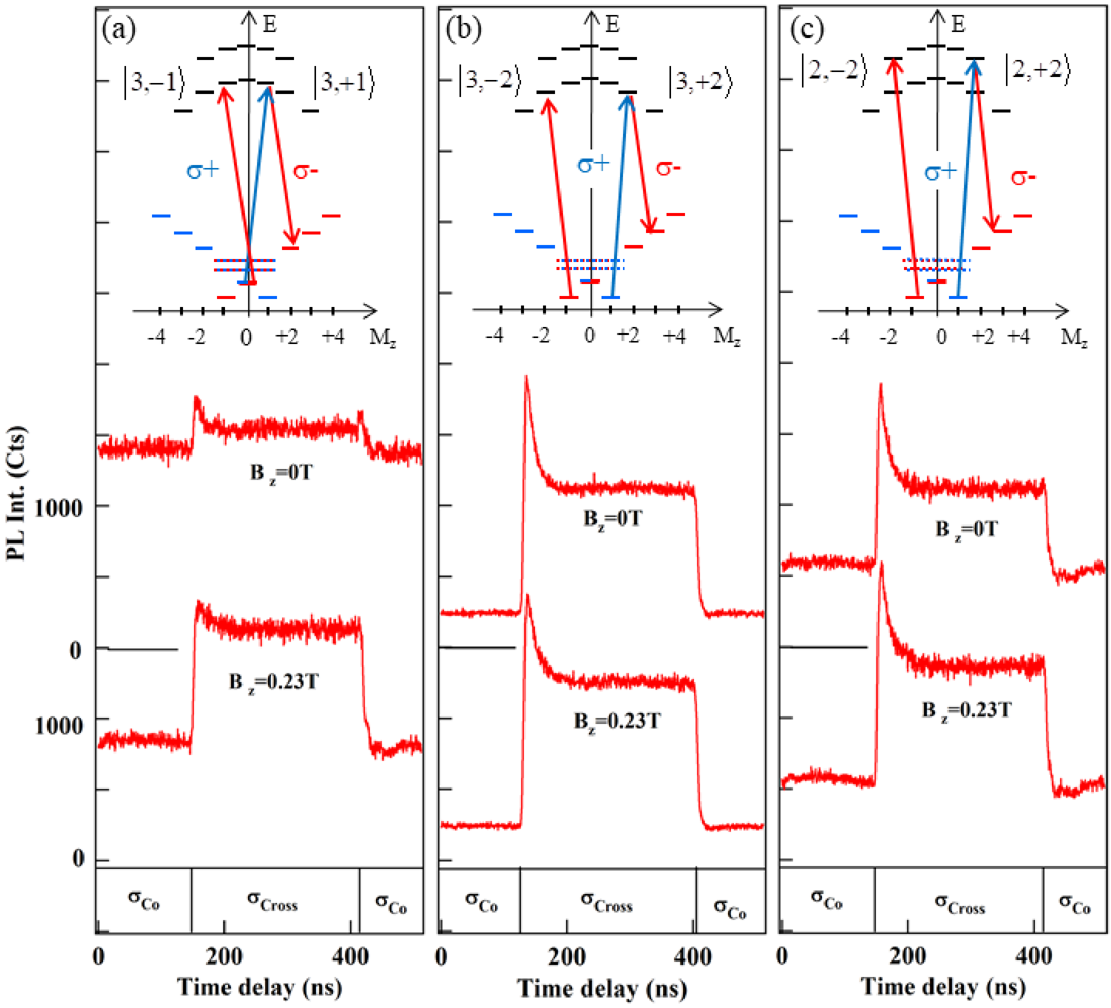

Figure I.8: Resonant optical pumping transients obtained under circular polarization switching of the resonant excitation for the Λ systems associated with (a) $|3,+1\rangle$, (b) $|3,+2\rangle$ and (c) $|2,+2\rangle$ at zero field and under a weak longitudinal magnetic field B_z=0.23T. The insets present the corresponding states which are resonantly excited and detected in $\sigma-$ polarization.

the co and cross circularly polarized resonant PL intensities are identical (see the inset of Fig. I.13 (b)) and similar pumping transients are observed when switching from σ_{co} to σ_{cross} or from σ_{cross} to σ_{co} circular polarization.

To observe the relaxation of the prepared non–equilibrium distribution of the Mn-hole spins, the circularly polarized pump laser is switched off during a dark time τ_{dark}. The amplitude of the pumping transient which appears after τ_{dark} depends on the Mn-hole spin relaxation. A dark time of 50 ns is enough to observe

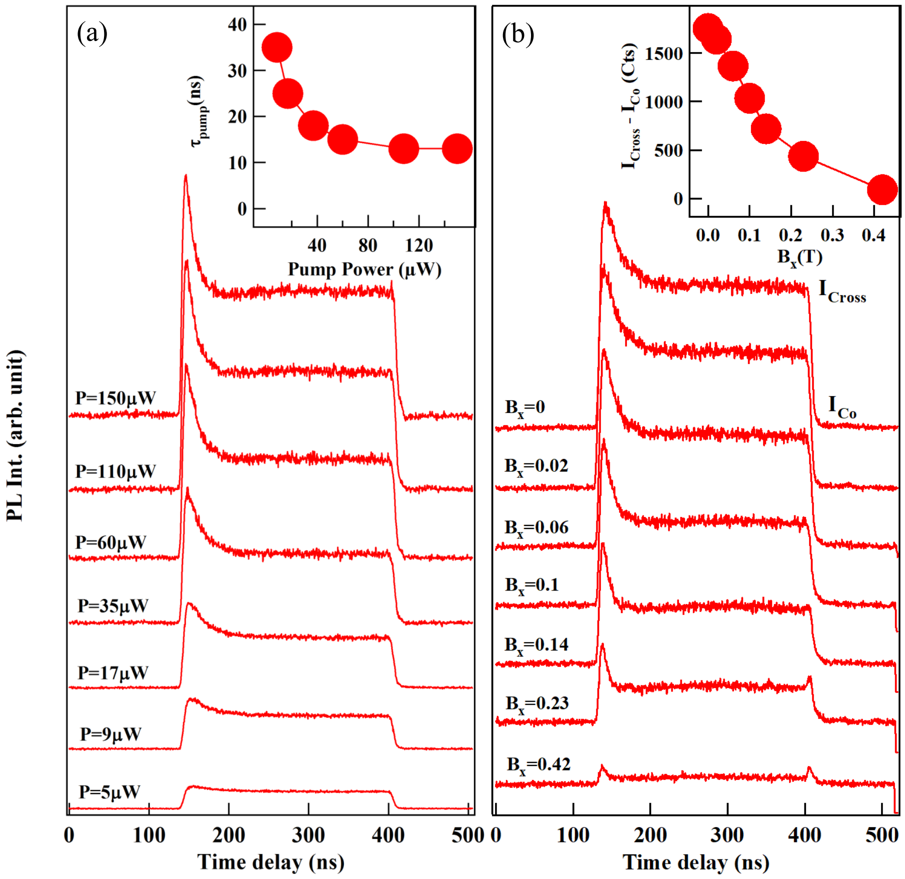

Figure I.9: Excitation power dependence (a) and transverse magnetic field dependence (b) of the optical pumping signal obtained for a resonant excitation on $|3, +2\rangle$. Insets: excitation power dependence of the pumping time and transverse magnetic field dependence of the difference of resonant PL intensity between a σ_{cross} and a σ_{co} excitation.

the reappearance of a significant pumping transient (Fig. ??). For comparison and for a better sensitivity of the measurement, the pumping transient observed in the absence of initial preparation of the Mn-hole spin (i.e. when switching of the circular polarization during the dark time) is also presented (red trace in Fig. I.10). The normalized difference of the amplitude of these two transients, $\Delta I/I$, as a function of τ_{dark} is presented in the inset of Fig.I.10. This measurement shows that, when the optical excitation is off, it takes around 80 ns to the Mn-hole spin to come back to the ground state of the excited Λ system.

If the optical pumping was storing the Mn-hole spin in the branch of the Λ system which is not optically excited, its characteristic time would be controlled by

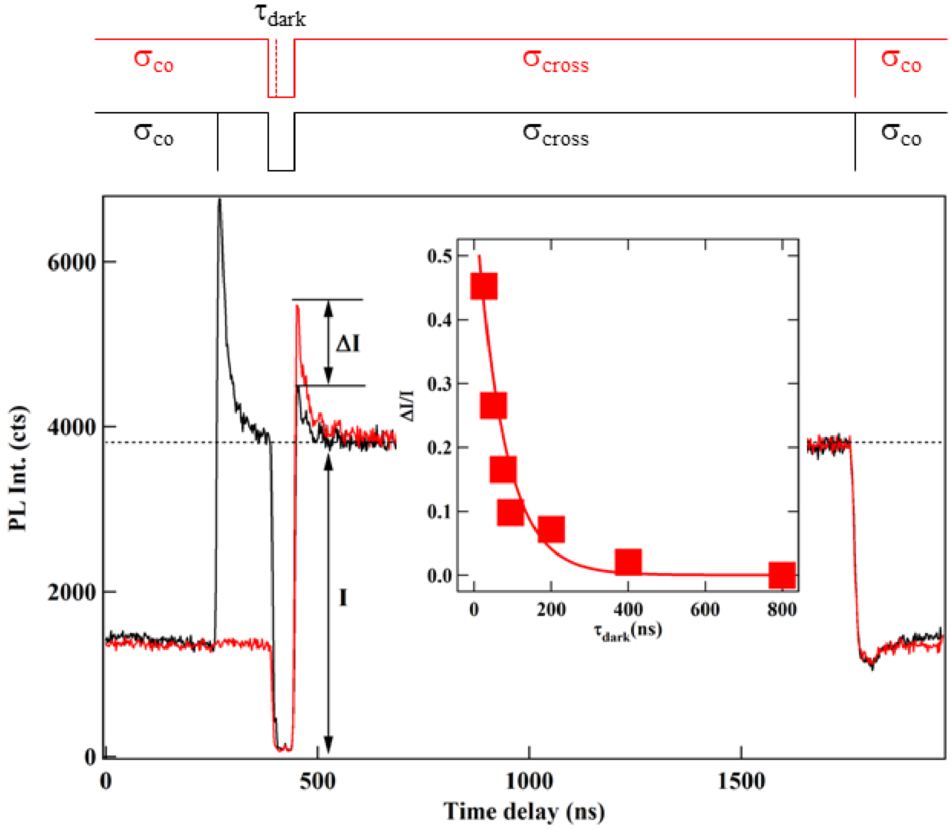

Figure I.10: Optical pumping experiment for an excitation of $|3,+2\rangle$ with modulated circular polarization. A dark time ($\tau_{dark} = 50ns$) is introduced in the pumping sequence. The polarization switching occurs either before (black) or during (red) the dark time. The black and red diagrams present the corresponding resonant excitation sequences. The inset presents the variation of the ratio $\Delta I/I$ as a function of τ_{dark}. The solid line is an exponential fit with $\tau_{relax} = 80ns$.

the exciton radiative lifetime and the generation rate. With a Mn-hole relaxation time in the 100 ns range, as observed experimentally, the pumping should take place within a few nanoseconds.

Another source of spin pumping can be the leak outside the resonantly excited Λ system. In this case, the speed of the pumping is controlled by the leakage time and, as observed experimentally, the pumping time is similar to the width of the photon bunching signal. This mechanism of pumping for the Mn-hole spin is confirmed by the transverse magnetic field dependence. The acceleration of the optical pumping in transverse magnetic field (Fig. I.9 (b)) has the same origin as the decrease of the width of the bunching signal. By mixing the different electron-Mn states, the transverse field enhances the leakage probability out of the resonantly driven Λ system and decreases the corresponding optical pumping time.

I.2.2 Relaxation mechanism

Hole-Mn flip-flops mediated by a lattice deformation

The observed large resonant PL amplitude of X$^+$-Mn and its dynamics can be qualitatively explained if a fast (nanosecond) and efficient spin transfer mechanism connects the two Mn-hole ground states of each Λ system. Let us note that efficient Mn-hole flip-flops are also required to explain the resonant luminescence observed on neutral Mn-doped QDs (see Appendix A).

We propose a mechanism for the Mn-hole flip-flop at low temperature resulting from a deformation induced exchange interaction [4, 5]. We show here that Mn-hole states are efficiently coupled via the interplay of their exchange interaction and the lattice deformation induced heavy-hole/light-hole mixing. We will focus in the following on the two Mn-hole states $|+\frac{3}{2};\Uparrow_h\rangle$ and $|+\frac{5}{2};\Downarrow_h\rangle$ in the ground states of the Λ system associated with the electron-Mn levels $|3,+2\rangle$ and $|2,+2\rangle$. Similar results could be obtained with the Mn-hole ground states of the other Λ systems.

First, let us notice that the non diagonal term of the Mn-hole exchange interaction $I_{hMn}/2(S^+J^- + S^-J^+)$ couples the heavy-holes $(\Uparrow_h, \Downarrow_h)$ and light-holes $(\uparrow_h, \downarrow_h)$ levels split by Δ_{lh} through a Mn-hole flip-flop. We consider this interaction as a perturbation on the Mn heavy-hole level structure given by $I_{hMn}S_zJ_z$. To the first order in I_{hMn}/Δ_{lh}, the two perturbed ground states of the Λ system considered here $\widetilde{|+\frac{3}{2};\Uparrow_h\rangle}$ and $\widetilde{|+\frac{5}{2};\Downarrow_h\rangle}$ can be written [6]:

$$
\begin{aligned}
\widetilde{|+\frac{5}{2};\Downarrow_h\rangle} &= |+\frac{5}{2};\Downarrow_h\rangle - \frac{\sqrt{15}}{2}\frac{I_{hMn}}{\Delta_{lh}}|+\frac{3}{2};\downarrow_h\rangle \\
\widetilde{|+\frac{3}{2};\Uparrow_h\rangle} &= |+\frac{3}{2};\Uparrow_h\rangle - \frac{\sqrt{15}}{2}\frac{I_{hMn}}{\Delta_{lh}}|+\frac{5}{2};\uparrow_h\rangle
\end{aligned}
$$

where we neglect the exchange energy shifts of the Mn-hole levels much smaller than Δ_{lh}.

Phonon-induced deformations comes into play via the off-diagonal terms of the Bir-Pikus Hamiltonian $\mathcal{H}_{BP}$, describing the influence of strain on the valence band, as written in Eq. ??. The parameters a_ν, b and d are given in Tab. I.2. The strain produced by phonon vibrations couples the perturbed Mn-hole states $\widetilde{|+5/2\Downarrow_h\rangle}$

Table I.2: Material (CdTe or ZnTe) [7] and QD parameters used in the calculation of the coupled hole and Mn spin relaxation time.

CdTe		
Deformation potential constants	b	-1.0 eV
	d	-4.4 eV
Longitudinal sound speed	c_l	3300 m/s
Transverse sound speed	c_t	1800 m/s
Density	ρ	5860 kg/m^3
ZnTe		
Deformation potential constants	b	-1.4 eV
	d	-4.4 eV
Longitudinal sound speed	c_l	3800 m/s
Transverse sound speed	c_t	2300 m/s
Density	ρ	5908 kg/m^3
Quantum dot		
Hole Mn exchange energy	I_{hMn}	0.35 meV
hh-lh exciton splitting	Δ_{lh}	15 meV
Hole wave function widths:		
- in plane	$l_\perp$	3.0 nm
- z direction	l_z	1.25 nm

and $|+\widetilde{3/2}\Uparrow_h\rangle$ through the Hamiltonian term

$$\langle+\widetilde{\frac{5}{2};\Downarrow_h}|H_{BP}|+\widetilde{\frac{3}{2};\Uparrow_h}\rangle = 2\times(-\frac{\sqrt{15}}{2}\frac{I_{hMn}}{\Delta_{lh}})\times R^* \tag{I.3}$$

with

$$R = \frac{\sqrt{3}}{2}b(\epsilon_{xx}-\epsilon_{yy}) - id\epsilon_{xy} \tag{I.4}$$

a deformation dependent non-diagonal term of $\mathcal{H}_{BP}$ [4, 5]. The coupling of the Mn-hole states is a result of an interplay between the Mn-hole exchange interaction and the deformation: neither the exchange interaction nor the deformation perturbation alone can couple these states.

According to (I.3), an effective Hamiltonian describing the discussed interaction mechanism with phonons in the subspace $\{|+\frac{5}{2};\Uparrow_h\rangle, |+\frac{5}{2};\Downarrow_h\rangle, |+\frac{3}{2};\Uparrow_h\rangle, |+\frac{3}{2};\Downarrow_h\rangle\}$ is

$$H_{int} = -\sqrt{15}\frac{I_{hMn}}{\Delta_{lh}}R^*|+\frac{5}{2};\Downarrow_h\rangle\langle+\frac{3}{2};\Uparrow_h|+H.c \tag{I.5}$$

The spin decay rates from $|+\frac{3}{2};\Uparrow_h\rangle$ to $|+\frac{5}{2};\Downarrow_h\rangle$ accompanied by the emission of an acoustic phonon is then given by Fermi's golden rule

$$\tau^{-1} = \frac{2\pi}{\hbar}\sum_k \left|\langle +\frac{5}{2};\Downarrow_h;\psi;n_k+1|H_{int}|+\frac{3}{2};\Uparrow_h;\psi;n_k\rangle\right|^2 \times \delta(\hbar\omega_0 - \hbar\omega_k)$$

where $\hbar\omega_0$ is the energy splitting between $|+\frac{5}{2};\Downarrow_h\rangle$ and $|+\frac{3}{2};\Uparrow_h\rangle$, n_k the number of phonons in mode k and ψ the orbital part of the hole wave function.

To evaluate the matrix element in (**??**) we use the strain tensor components ϵ_{ij} given by

$$\epsilon_{ij} = \frac{1}{2}\left(\frac{\partial u_i}{\partial r_j} + \frac{\partial u_j}{\partial r_i}\right) \tag{I.6}$$

where $\overrightarrow{u}(\overrightarrow{r})$ is the local displacement field. For an acoustic phonon, the quantized displacement field can be written in the real space [5, 8]:

$$\overrightarrow{u}(\overrightarrow{r}) = i\sum_{k,\lambda}\sqrt{\frac{\hbar}{2\rho\omega_{k,\lambda}N\nu_0}}\overrightarrow{e}_{k,\lambda}(b_{k,\lambda} + b^\dagger_{-k,\lambda})e^{i\overrightarrow{k}\overrightarrow{r}} \tag{I.7}$$

where N is the number of unit cells in the crystal, ν_0 is the volume of a cell and ρ the mass density. $b^\dagger_{k,\lambda}$ $(b_{k,\lambda})$ is the creation (annihilation) operator of phonon in the mode (k,λ) of energy $\hbar\omega_{k\lambda}$ and unit polarization vector $\overrightarrow{e}_{k,\lambda}$. In zinc-blend crystals there are two transverse acoustic phonon branches $\lambda = t_1, t_2$ and one longitudinal acoustic phonon branch $\lambda = l$. The polarization vectors of these phonons branches are given by [9]

$$\begin{array}{rcl} \overrightarrow{e}_{k,l} &=& \frac{\overrightarrow{k}}{k} = \frac{1}{k}(k_x,k_y,k_z) \\ \overrightarrow{e}_{k,t_1} &=& \frac{1}{kk_\perp}(k_xk_z,k_yk_z,-k_\perp^2) \\ \overrightarrow{e}_{k,t_2} &=& \frac{1}{k_\perp}(k_y,-k_x,0) \end{array} \tag{I.8}$$

with $k_\perp = \sqrt{k_x^2+k_y^2}$.

Upon substitutions given by (I.6), (I.7) and (I.8), we obtain for the matrix element in (**??**):

$$\begin{array}{rl} |M_{k,\lambda}|^2 = & 15\left(\frac{I_{hMn}}{\Delta_{lh}}\right)^2 \frac{\hbar}{2\rho\omega_{k,\lambda}N\nu_0}\left(n_B(\omega_{k,\lambda})+1\right) \\ & \times\left(\frac{3b^2}{4}(k_xe_{x,\lambda}-k_ye_{y,\lambda})^2 + \frac{d^2}{4}(k_xe_{y,\lambda}+k_ye_{x,\lambda})^2 \times |\mathcal{F}_\lambda(\overrightarrow{k})|^2\right. \end{array} \tag{I.9}$$

with

$$\mathcal{F}_\lambda(\overrightarrow{k}) = \int_{-\infty}^{\infty} d^3r\psi^*(\overrightarrow{r})e^{i\overrightarrow{k}\overrightarrow{r}}\psi(\overrightarrow{r}) \tag{I.10}$$

and $n_B(\omega_{k,\lambda}) = 1/(e^{\hbar\omega_{k,\lambda}/K_BT} - 1)$, the thermal phonon distribution function.

For a Gaussian hole wave function with in-plane and z-direction parameters $l_\perp$ and l_z respectively (full width at half maximum $2\sqrt{2\ln 2}l_i$)

$$\psi(\overrightarrow{r}) = \frac{1}{\pi^{3/4} l_\perp \sqrt{l_z}} e^{-\frac{1}{2}\left(\left(\frac{r_\perp}{l_\perp}\right)^2 + \left(\frac{z}{l_z}\right)^2\right)} \tag{I.11}$$

the form factor $\mathcal{F}_\lambda(\overrightarrow{k})$, which is the Fourier transform of $|\psi(\overrightarrow{r})|^2$, becomes

$$\mathcal{F}_\lambda(\overrightarrow{k}) = e^{-\frac{1}{4}\left((l_\perp k_\perp)^2 + (l_z k_z)^2\right)} \tag{I.12}$$

Considering a linear dispersion of acoustic phonons $\omega_{k,\lambda} = c_\lambda k$ and in spherical coordinates with $\overrightarrow{k} = k(\sin\theta\cos\varphi, \sin\theta\sin\varphi, \cos\theta)$, the explicit formula of the decay rate (**??**) is

$$\begin{aligned} \tau^{-1} = \; & \sum_\lambda \frac{15}{(2\pi)^2} \left(\frac{I_{hMn}}{\Delta_{lh}}\right)^2 \left(\frac{\omega_0}{c_\lambda}\right)^3 \frac{1}{2\hbar\rho c_\lambda^2} \frac{\pi}{4} (3b^2 + d^2) \\ & \times (n_B(\omega_0) + 1)) \int_0^\pi d\theta \sin\theta |\mathcal{F}_\lambda(\omega_0, \theta)|^2 G_\lambda(\theta) \end{aligned} \tag{I.13}$$

where we used the continuum limit ($\sum_k \rightarrow V/(2\pi)^3 \int d^3k$ with $V = N\nu_0$ the crystal volume) and integrated over k and φ. The summation is taken over the acoustic phonon branches λ of corresponding sound velocity c_λ. The geometrical form factors for each phonon branch, $G_\lambda(\theta)$, are given by

$$\begin{aligned} G_l(\theta) = \; & \sin^4\theta \\ G_{t_1}(\theta) = \; & \sin^2\theta\cos^2\theta \\ G_{t_2}(\theta) = \; & \sin^2\theta \end{aligned} \tag{I.14}$$

In the numerical calculation of the spin flip time τ_{ff} presented in Fig.I.11 we use the material parameters of CdTe or ZnTe and the typical parameters for self-assembled CdTe/ZnTe QDs listed in Table I.2. The calculated relaxation time strongly depend on the energy separation between the Mn-hole levels $\hbar\omega_0$. This energy dependence is controlled by the size of the hole wave-function given by $l_\perp$ and l_z. The estimated flip-flop time is also strongly sensitive on the exchange induced mixing of the ground heavy-hole states with the higher energy light-hole levels. In our model, this mixing is controlled by Δ_{lh}, an effective energy splitting between heavy-holes and light-holes. This simple parameter can indeed describe more complex effects such as a coupling of the confined heavy-hole with ground state light-holes in the barriers [10] or effective reduction of heavy-hole/light-hole splitting due to a presence of a dense manifold of heavy-hole like QD states lying between the confined heavy-hole and light-hole levels [11]. From this modelling we deduce that for a hole confined in small $Cd_xZn_{1-x}Te$ alloy QDs, the Mn-hole

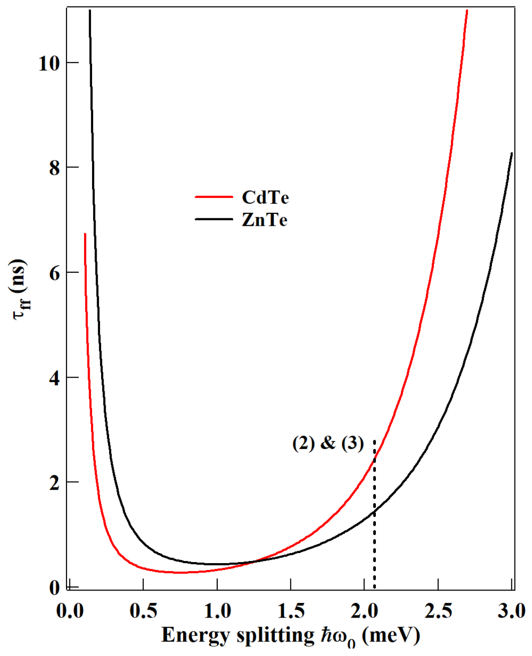

Figure I.11: Relaxation time τ_{ff}, between the two Mn-hole ground states of the Λ system calculated with the material and QD parameters listed in Table I.2 and a temperature T=7K. The vertical line shows the energy splitting in the studied QD of the Mn-hole states involved in the Λ systems considered here (Resonances (2) and (3) identified in Fig. I.4).

flip-flop time τ_{ff} can be easily bellow 2 ns for an effective heavy-hole/light-hole splitting Δ_{lh}=15 meV and an energy separation in the meV range, typical for the Mn-hole spin splitting in magnetic QDs. We will use in the following calculations τ_{ff}=1.5 ns for the ground states of each Λ system.

Model of the carrier-Mn spin dynamics under resonant excitation

Sed mattis, erat sit amet gravida malesuada, elit augue egestas diam, tempus scelerisque nunc nisl vitae libero. Sed consequat feugiat massa. Nunc porta, eros in eleifend varius, erat leo rutrum dui, non convallis lectus orci ut nibh. Sed lorem massa, nonummy quis, egestas id, condimentum at, nisl. Maecenas at nibh. Aliquam et augue at nunc pellentesque ullamcorper. Duis nisl nibh, laoreet suscipit, convallis ut, rutrum id, enim. Phasellus odio. Nulla nulla elit, molestie non, scelerisque at, vestibulum eu, nulla. Ut odio nisl, facilisis id, mollis et, scelerisque nec, enim. Aenean sem leo, pellentesque sit amet, scelerisque sit amet, vehicula pellentesque, sapien.

Phasellus id magna. Duis malesuada interdum arcu. Integer metus. Morbi pulvinar pellentesque mi. Suspendisse sed est eu magna molestie egestas. Quisque mi lorem, pulvinar eget, egestas quis, luctus at, ante. Proin auctor vehicula purus. Fusce ac nisl aliquam ante hendrerit pellentesque. Class aptent taciti sociosqu ad litora torquent per conubia nostra, per inceptos hymenaeos. Morbi wisi. Etiam

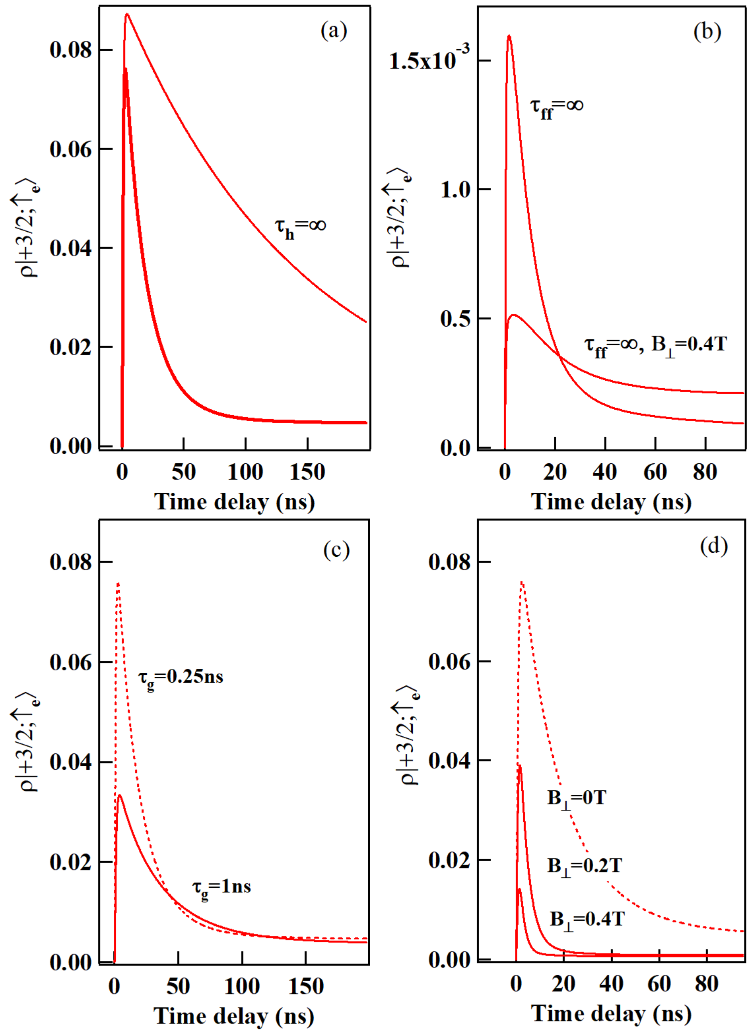

Figure I.12: (a) Calculated time evolution of $\rho_{|+\frac{3}{2},\uparrow_e\rangle}(t)$ with the QD parameters listed in Table I.1 and (unless specified) τ_r=0.3ns, τ_{Mn}=5 μs, τ_h=10ns, τ_g=0.25 ns, τ_{ff}=1.5 ns, T_2^{hMn}= 5 ns, T_2^{eMn}= 0.5 ns, T=10K and B$_\perp$=0. (b) (c) and (d) illustrate the influence of, respectively, τ_{ff}, τ_g and $B_\perp$ on $\rho_{|+\frac{3}{2},\uparrow_e\rangle}(t)$. Note the different vertical scale in (b).

arcu mauris, facilisis sed, eleifend non, nonummy ut, pede. Cras ut lacus tempor metus mollis placerat. Vivamus eu tortor vel metus interdum malesuada.

Nullam eleifend justo in nisl. In hac habitasse platea dictumst. Morbi nonummy. Aliquam ut felis. In velit leo, dictum vitae, posuere id, vulputate nec, ante. Maecenas vitae pede nec dui dignissim suscipit. Morbi magna. Vestibulum id purus eget velit laoreet laoreet. Praesent sed leo vel nibh convallis blandit.

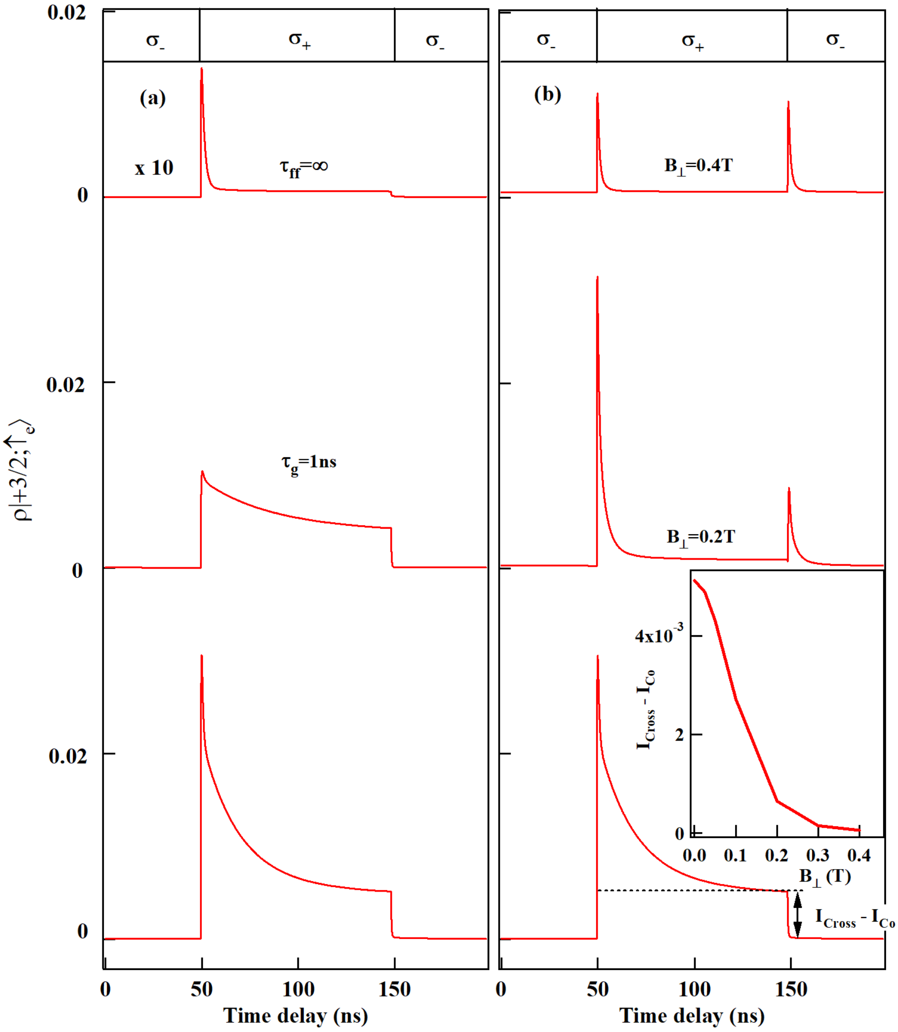

Figure I.13: Calculated resonant optical pumping transients for a $\sigma-$ detection and an excitation of $|3,+2\rangle$ and $|3,-2\rangle$ with modulated circular polarization. The QD parameters for the calculations are those listed in table I.1 and τ_r=0.3 ns, τ_{Mn}=5 μs, τ_h=10 ns, T_2^{hMn}= 5 ns, T_2^{eMn}= 0.5 ns, τ_{ff}=1.5 ns, T=10 K and τ_g=0.25 ns. (a) Influence of a variation of τ_g and τ_{ff}. (b) Influence of a transverse magnetic field $B_\perp$. The inset presents the transverse magnetic field dependence of the difference of population for a $\sigma+$ or a $\sigma-$ excitation.

Ut rutrum. Donec nibh. Donec interdum. Fusce sed pede sit amet elit rhoncus ultrices. Nullam at enim vitae pede vehicula iaculis.

Class aptent taciti sociosqu ad litora torquent per conubia nostra, per inceptos hymenaeos. Aenean nonummy turpis id odio. Integer euismod imperdiet turpis.

Ut nec leo nec diam imperdiet lacinia. Etiam eget lacus eget mi ultricies posuere. In placerat tristique tortor. Sed porta vestibulum metus. Nulla iaculis sollicitudin pede. Fusce luctus tellus in dolor. Curabitur auctor velit a sem. Morbi sapien. Class aptent taciti sociosqu ad litora torquent per conubia nostra, per inceptos hymenaeos. Donec adipiscing urna vehicula nunc. Sed ornare leo in leo. In rhoncus leo ut dui. Aenean dolor quam, volutpat nec, fringilla id, consectetuer vel, pede.

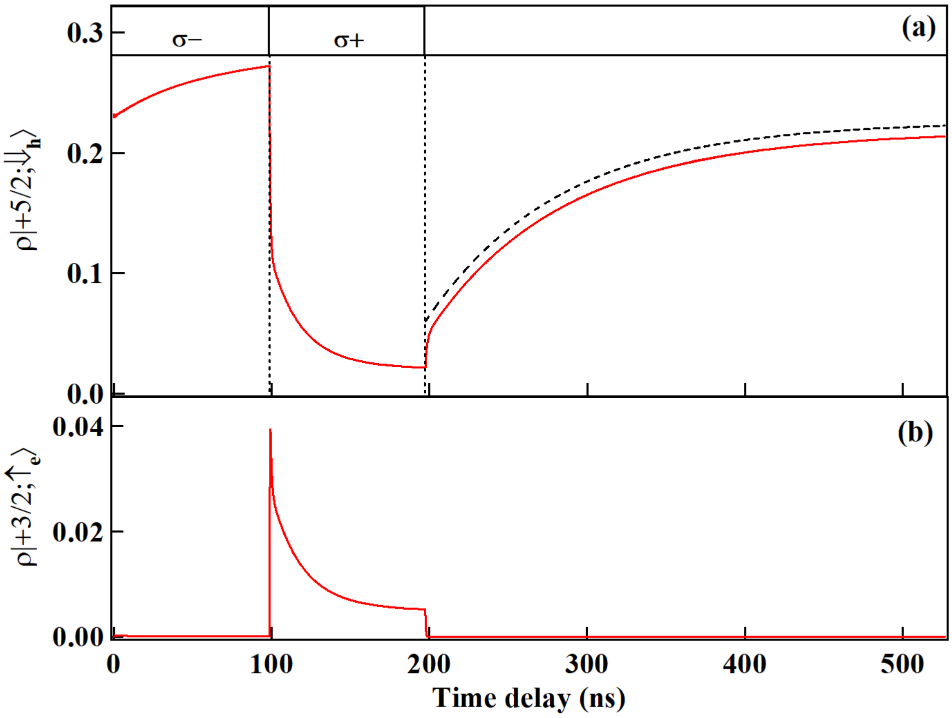

Figure I.14: (a) Calculated time evolution in the dark of the population of the hole-Mn state $|+\frac{5}{2}, \Downarrow_h\rangle$ initialized by a sequence of $\sigma-/\sigma+$ resonant excitation of $|3,-2\rangle$ and $|3,+2\rangle$. The dashed black line (shifted for clarity) is an exponential fit with a characteristic time τ_{relax}=85 ns. (b) Corresponding calculated time evolution of the population $|+\frac{3}{2}, \uparrow_e\rangle$. The parameters are those of Fig. I.13.

Nulla malesuada risus ut urna. Aenean pretium velit sit amet metus. Duis iaculis. In hac habitasse platea dictumst. Nullam molestie turpis eget nisl. Duis a massa id pede dapibus ultricies. Sed eu leo. In at mauris sit amet tortor bibendum varius. Phasellus justo risus, posuere in, sagittis ac, varius vel, tortor. Quisque id enim. Phasellus consequat, libero pretium nonummy fringilla, tortor lacus vestibulum nunc, ut rhoncus ligula neque id justo. Nullam accumsan euismod nunc. Proin vitae ipsum ac metus dictum tempus. Nam ut wisi. Quisque tortor felis, interdum ac, sodales a, semper a, sem. Curabitur in velit sit amet dui tristique sodales. Vivamus mauris pede, lacinia eget, pellentesque quis, scelerisque eu, est. Aliquam risus. Quisque bibendum pede eu dolor.

Donec tempus neque vitae est. Aenean egestas odio sed risus ullamcorper ullamcorper. Sed in nulla a tortor tincidunt egestas. Nam sapien tortor, elementum sit amet, aliquam in, porttitor faucibus, enim. Nullam congue suscipit nibh. Quisque convallis. Praesent arcu nibh, vehicula eget, accumsan eu, tincidunt a, nibh. Suspendisse vulputate, tortor quis adipiscing viverra, lacus nibh dignissim tellus, eu suscipit risus ante fringilla diam. Quisque a libero vel pede imperdiet aliquet. Pellentesque nunc nibh, eleifend a, consequat consequat, hendrerit nec, diam. Sed urna. Maecenas laoreet eleifend neque. Vivamus purus odio, eleifend non, iaculis a, ultrices sit amet, urna. Mauris faucibus odio vitae risus. In nisl. Praesent purus. Integer iaculis, sem eu egestas lacinia, lacus pede scelerisque augue, in ullamcorper dolor eros ac lacus. Nunc in libero.

Fusce suscipit cursus sem. Vivamus risus mi, egestas ac, imperdiet varius, faucibus quis, leo. Aenean tincidunt. Donec suscipit. Cras id justo quis nibh scelerisque dignissim. Aliquam sagittis elementum dolor. Aenean consectetuer justo in pede. Curabitur ullamcorper ligula nec orci. Aliquam purus turpis, aliquam id, ornare vitae, porttitor non, wisi. Maecenas luctus porta lorem. Donec vitae ligula eu ante pretium varius. Proin tortor metus, convallis et, hendrerit non, scelerisque in, urna. Cras quis libero eu ligula bibendum tempor. Vivamus tellus quam, malesuada eu, tempus sed, tempor sed, velit. Donec lacinia auctor libero.

Morbi justo. Aenean nec dolor. In hac habitasse platea dictumst. Proin nonummy porttitor velit. Sed sit amet leo nec metus rhoncus varius. Cras ante. Vestibulum commodo sem tincidunt massa. Nam justo. Aenean luctus, felis et condimentum lacinia, lectus enim pulvinar purus, non porta velit nisl sed eros. Suspendisse consequat. Mauris a dui et tortor mattis pretium. Sed nulla metus, volutpat id, aliquam eget, ullamcorper ut, ipsum. Morbi eu nunc. Praesent pretium. Duis aliquam pulvinar ligula. Ut blandit egestas justo. Quisque posuere metus viverra pede.

Vivamus sodales elementum neque. Vivamus dignissim accumsan neque. Sed at enim. Vestibulum nonummy interdum purus. Mauris ornare velit id nibh pretium ultricies. Fusce tempor pellentesque odio. Vivamus augue purus, laoreet in, scelerisque vel, commodo id, wisi. Duis enim. Nulla interdum, nunc eu semper eleifend, enim dolor pretium elit, ut commodo ligula nisl a est. Vivamus ante. Nulla leo massa, posuere nec, volutpat vitae, rhoncus eu, magna.

Quisque facilisis auctor sapien. Pellentesque gravida hendrerit lectus. Mauris rutrum sodales sapien. Fusce hendrerit sem vel lorem. Integer pellentesque massa vel augue. Integer elit tortor, feugiat quis, sagittis et, ornare non, lacus. Vestibulum posuere pellentesque eros. Quisque venenatis ipsum dictum nulla. Aliquam

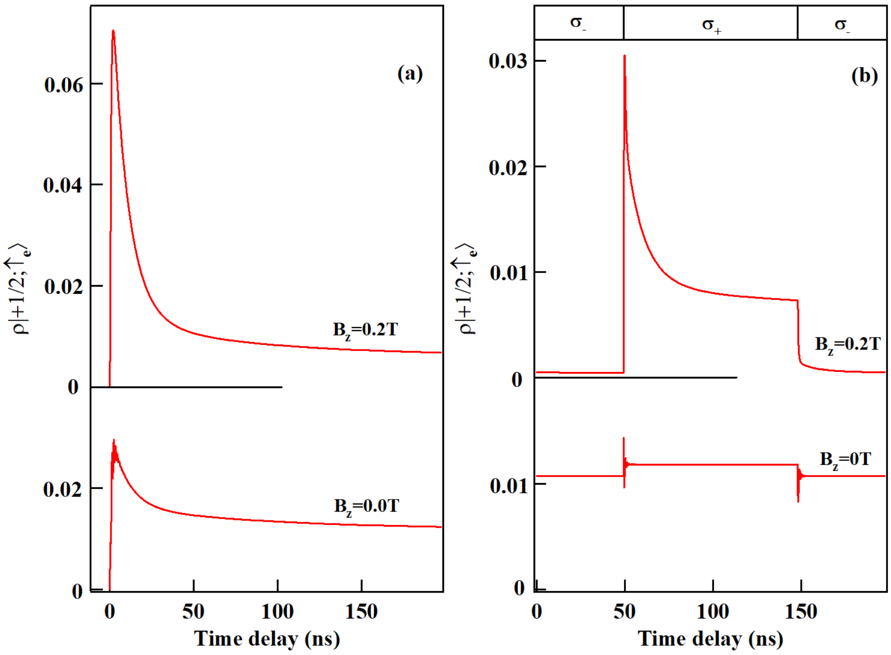

Figure I.15: (a) Calculated time evolution of $\rho_{|+\frac{1}{2},\uparrow_e\rangle}$ with $\rho_{|+\frac{1}{2},\Uparrow_h\rangle}$=1 (Mn-hole spin in the state $|+\frac{1}{2},\Uparrow_h\rangle$ after a $\sigma-$ recombination) for a resonant $\sigma+$ excitation of the coupled electron-Mn states $|3,+1\rangle$ and $|3,-1\rangle$ without and with a longitudinal magnetic field. (b) Time evolution of $\rho_{|+\frac{1}{2},\uparrow_e\rangle}$ under excitation with modulated circular polarization. The parameters used in the calculations are those of Fig. I.13.

quis quam non metus eleifend interdum. Nam eget sapien ac mauris malesuada adipiscing. Etiam eleifend neque sed quam. Nulla facilisi. Proin a ligula. Sed id dui eu nibh egestas tincidunt. Suspendisse arcu.

a

We saw the influence of strain anisotropy. We will now see a way to extract it more precisely.

I.3 Influence of the strain anisotropy

In hac habitasse platea dictumst. Proin at est. Curabitur tempus vulputate elit. Pellentesque sem. Praesent eu sapien. Duis elit magna, aliquet at, tempus sed, vehicula non, enim. Morbi viverra arcu nec purus. Vivamus fringilla, enim et commodo malesuada, tortor metus elementum ligula, nec aliquet est sapien ut lectus.

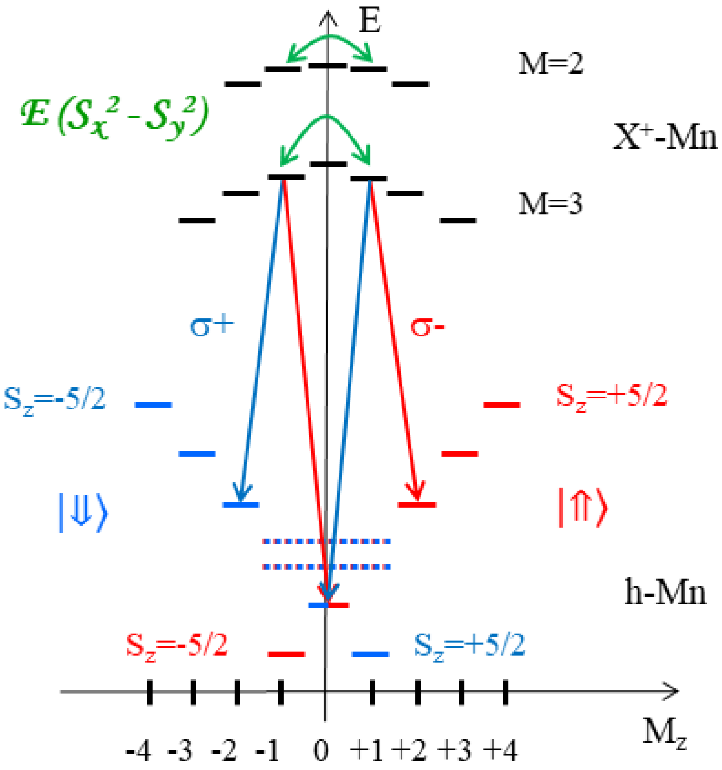

Figure I.16: Energy levels of the ground (h-Mn) and excited (X^+-Mn) states as a function of their angular momentum (M_z). The e-Mn states $|3,+1\rangle$ and $|3,-1\rangle$, as well as $|2,+1\rangle$ and $|2,-1\rangle$, are coupled by the strain anisotropy $E(S_x^2 - S_y^2)$. Optical Λ systems associated with $|3,+1\rangle$ and $|3,-1\rangle$ are presented.

Aliquam mi. Ut nec elit. Fusce euismod luctus tellus. Curabitur scelerisque. Nullam purus. Nam ultricies accumsan magna. Morbi pulvinar lorem sit amet ipsum. Donec ut justo vitae nibh mollis congue. Fusce quis diam. Praesent tempus eros ut quam.

Donec in nisl. Fusce vitae est. Vivamus ante ante, mattis laoreet, posuere eget, congue vel, nunc. Fusce sem. Nam vel orci eu eros viverra luctus. Pellentesque sit amet augue. Nunc sit amet ipsum et lacus varius nonummy. Integer rutrum sem eget wisi. Aenean eu sapien. Quisque ornare dignissim mi. Duis a urna vel risus pharetra imperdiet. Suspendisse potenti.

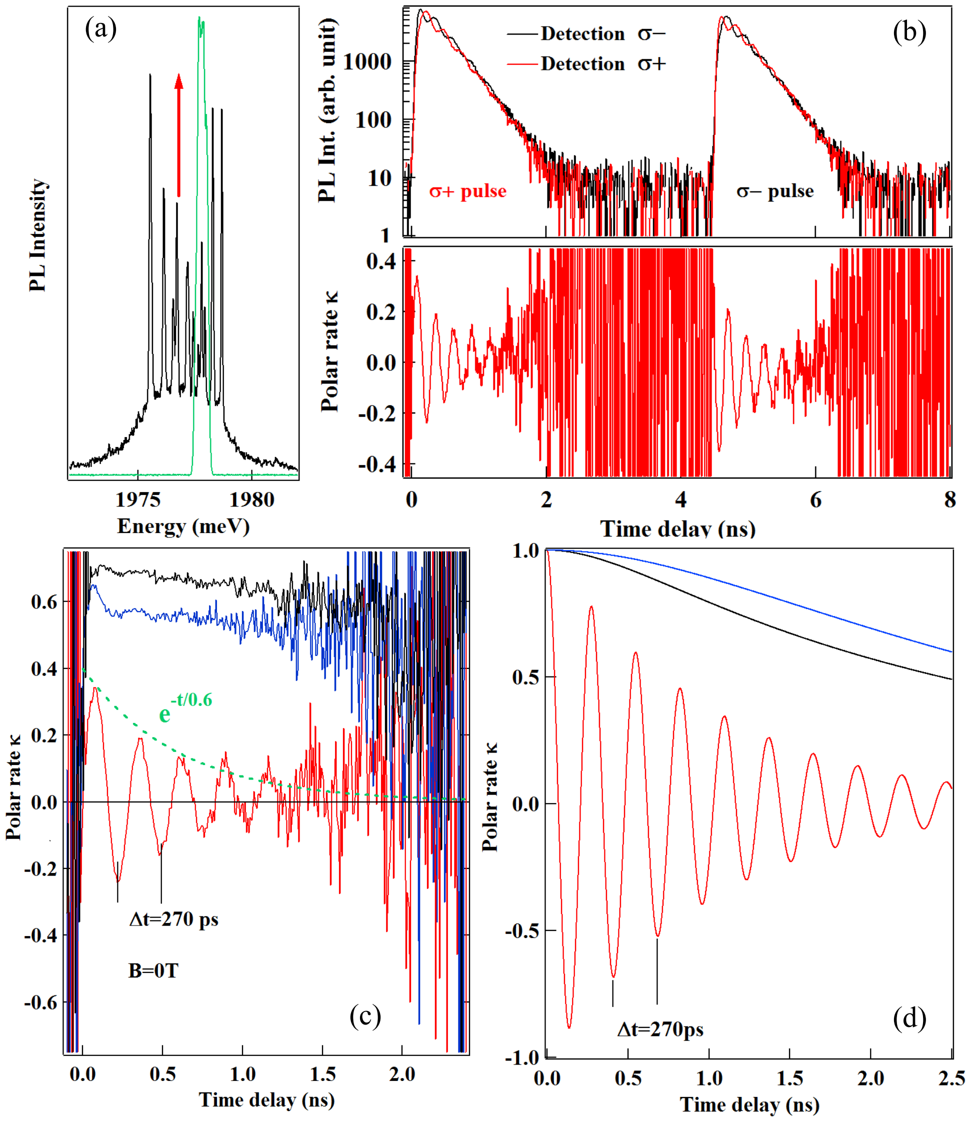

Figure I.17: (a) Configuration of the time resolved PL experiment for an excitation of $|3,+1\rangle$ (pulsed laser in green). (b) Top panel: Time resolved resonant PL of $|3,+1\rangle$ with a $\sigma+/\sigma-$ sequence of laser pulses and a detection in $\sigma+$ and $\sigma-$ polarization. Bottom panel: corresponding time dependence of the circular polarization rate $\kappa = (\sigma_- - \sigma_+)/(\sigma_- + \sigma_+)$. (c) Time dependence of the circular polarization rate of the resonant PL of the states $|3,+1\rangle$ (red), $|3,+2\rangle$ (black) and $|2,+2\rangle$ (blue). (d) Corresponding polarisation rates calculated with $D_0 = 7\mu eV$ [2], $T_2^{eMn} = 0.6ns$, $E = 1.8\mu eV$, a radiative lifetime $T_r = 0.3ns$ and the parameters listed on Table I.1.

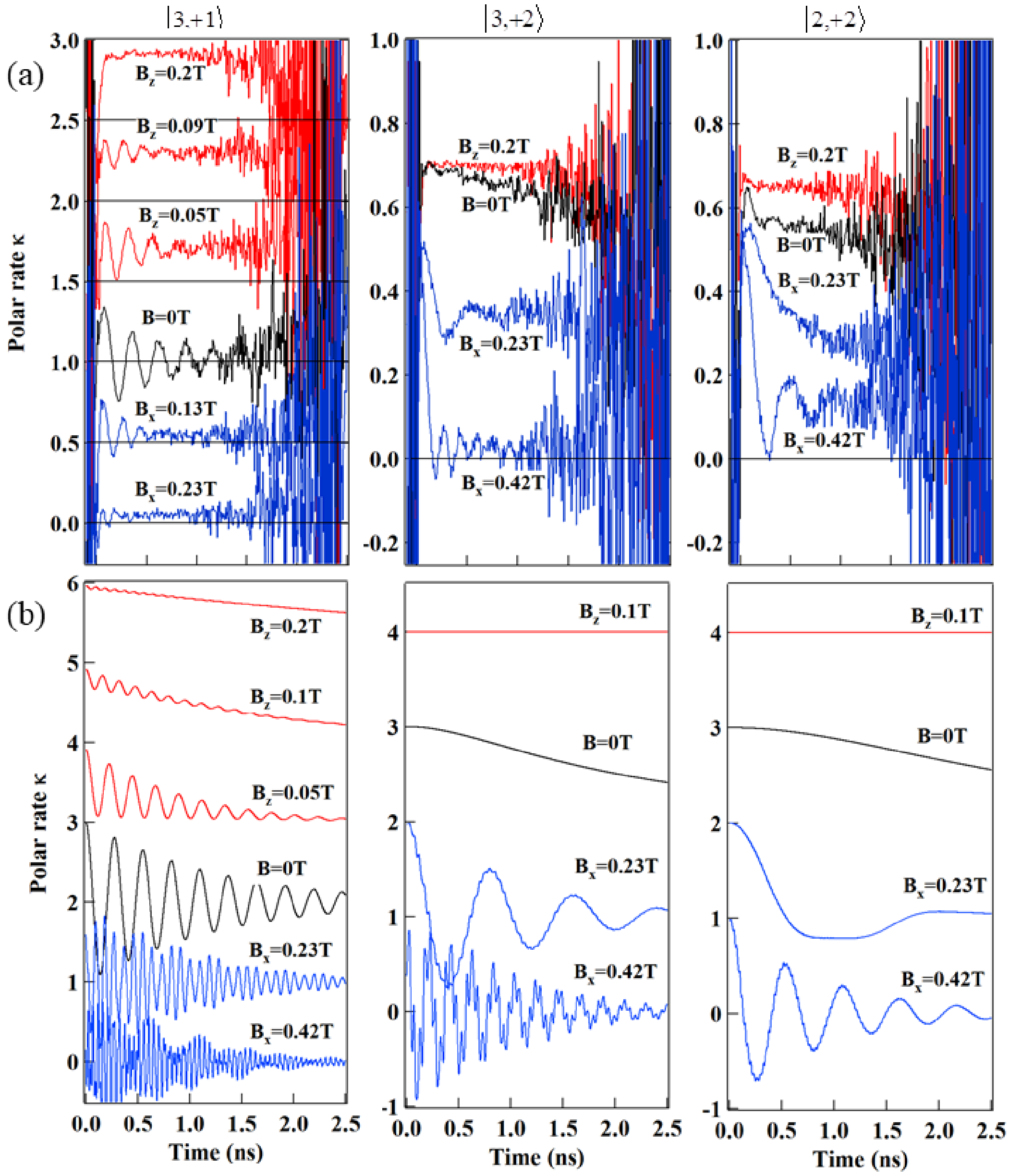

Figure I.18: (a) Influence of a longitudinal (B_z, red) and a transverse (B_x, blue) magnetic field on the time dependence of the circular polarization rate $\kappa = (\sigma_- - \sigma_+)/(\sigma_- + \sigma_+)$ of the resonant PL of $|3,+1\rangle$, $|3,+2\rangle$ and $|2,+2\rangle$. On the top left panel, curves are shifted by 0.5 for clarity. (b) Corresponding time dependence of the circular polarization rate calculated with $g_{Mn} = 2$, $g_e = -0.4$, $g_h = 0.6$ [2], and the parameters listed on Table I.1. The curves are shifted by 1 for clarity.

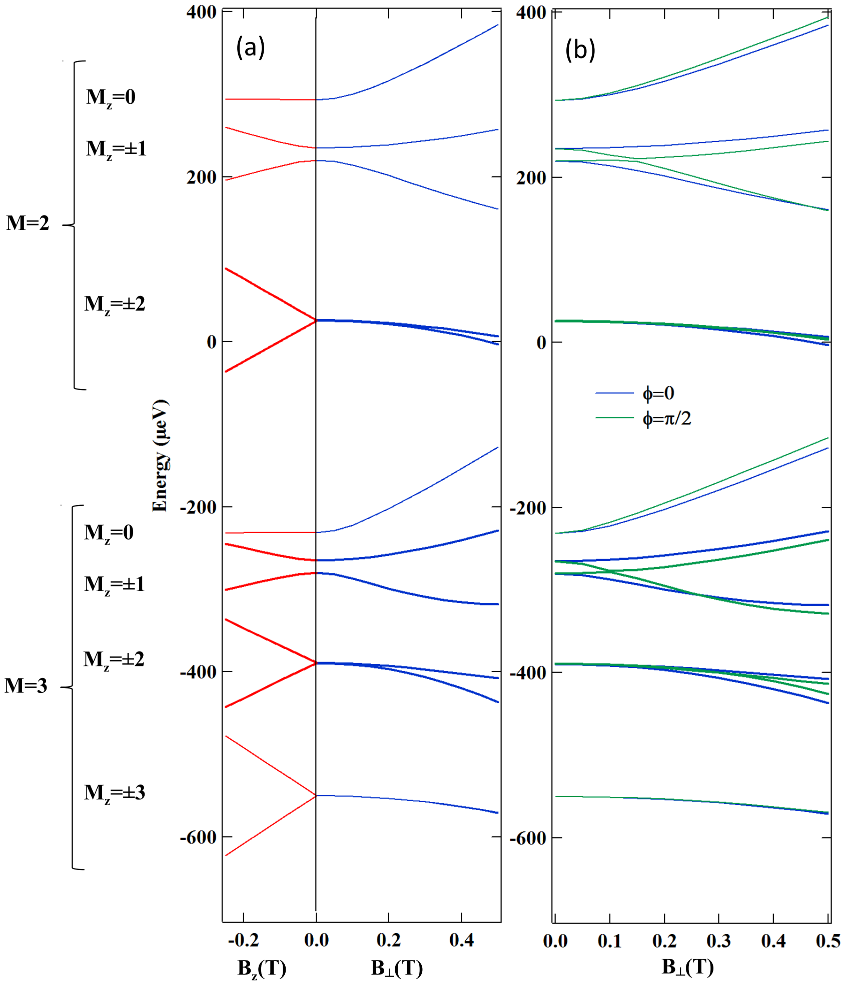

Figure I.19: (Color line) (a) Calculated energy of the electron-M, states in a longitudinal magnetic field (B_z) and in a transverse magnetic field ($B_\perp$). (b) Energy of the electron-Mn states for two orientations of the transverse magnetic field: $\phi = 0$ ($B_\perp = B_x$) $\phi = \frac{\pi}{2}$ ($B_\perp = B_y$). The parameters used in the calculations are listed in Table I.2, with the exception of E, for which the more precise value of 1.8 μeV was chosen.

Bibliography

[1] L. Besombes, H. Boukari, C. L. Gall, B. Brunetti, C. Cao, S. Jamet, and B. Varghese, "Optical control of the spin of a magnetic atom in a semiconductor quantum dot", Nanophotonics **4**, 75 (2015).

[2] B. Varghese, H. Boukari, and L. Besombes, "Dynamics of a Mn spin coupled to a single hole confined in a quantum dot", Phys. Rev. B **90**, 115307 (2014).

[3] L. Besombes, K. Kheng, L. Marsal, and H. Mariette, "Acoustic phonon broadening mechanism in single quantum dot emission", Phys. Rev. B **63**, 155307 (2001).

[4] E. Tsitsishvili, R. v. Baltz, and H. Kalt, "Exciton spin relaxation in single semiconductor quantum dots", Phys. Rev. B **67**, 205330 (2003).

[5] K. Roszak, V. M. Axt, T. Kuhn, and P. Machnikowski, "Exciton spin decay in quantum dots to bright and dark states", Phys. Rev. B **76**, 195324 (2007).

[6] C. Cohen-Tannoudji, B. Diu, and F. Laloe, *Mecanique quantique*, edited by P. Hermann (1973).

[7] S. Adachi, "Properties of group IV, II-V and II-VI semiconductors", in, edited by Wiley (2005) Chap. 8, p. 178.

[8] G. Mahan, *Many-particle physics*, edited by N. Y. Plenum Press (1993).

[9] L. M. Woods, T. L. Reinecke, and R. Kotlyar, "Hole spin relaxation in quantum dots", Phys. Rev. B **69**, 125330 (2004).

[10] P. Michler, *Single quantum dots fundamentals, applications and new concepts*, edited by B. Springer (2003).

[11] J.-W. Luo, G. Bester, and A. Zunger, "Supercoupling between heavy-hole and light-hole states in nanostructures", Phys. Rev. B **92**, 165301 (2015).